Geoderma 200–201 (2013) 140–155

Contents lists available at SciVerse ScienceDirect

Geoderma

journal homepage: www.elsevier.com/locate/geoderma

The use of Slingram EM38 data for topsoil and subsoil geoelectrical characterization with a Bayesian inversion

S. Grellier [a], N. Florsch [b,*], C. Camerlynck [c], J.L. Janeau [d], P. Podwojewski [e,f], S. Lorentz [f]

[a] University of Science and Technology of Hanoi, Viet Nam
[b] UPMC Univ. Paris 06, UMI 209 UMMISCO, F-75005, Paris, France
[c] UPMC Univ. Paris 06, UMR 7619 Sisyphe, F-75005, Paris, France
[d] IRD, UMR BIOEMCO c/o Soils and Fertilisers Research Institute, Hanoi, Viet Nam
[e] IRD, UMR 211 BIOEMCO, F-93143 Bondy cedex. France
[f] School of agriculture, Earth and Environmental Science, University of KwaZulu-Natal, South Africa

ARTICLE INFO

Article history:
Received 18 March 2012
Received in revised form 2 January 2013
Accepted 17 January 2013
Available online 22 March 2013

Keywords:
Topsoil
Soil conductivity
EM38
Slingram
Bayesian inversion
South Africa

ABSTRACT

We use the Bayesian method to invert a simple two-layer pedological horizon (1-D with a topsoil and a subsoil) of a surveyed site to be assessed. We show how the Bayesian method is well suited to the determination of topsoil/subsoil features, and can be used in particular as a tool for the analysis of parameters to be retrieved in terms of information content. Our approach is devoted mainly to the assessment of topsoil thickness, and of topsoil and subsoil conductivities, which are provided in terms of probability density functions. We first summarize the methodology implemented with the Geonics EM38-MK2 conductivity meter, and discuss the adaptation of field procedures and post-processing methods to mitigate the effects of drift and bias. We briefly review some non-Bayesian approaches, and then develop the Bayesian approach for the context of our geophysical survey, highlighting its merits. Positivity constraints (on thickness and conductivity) are included in the form of log parameters. A priori knowledge, based on an objective choice made by the geophysicist, is naturally included in the Bayesian scheme. We discuss the equivalence problem associated with the application of the Slingram method to soil structure analysis. The survey of a luvisol at the Kwazulu-Natal (South Africa) site of Potshini is used to illustrate an ecological application of the Slingram and Bayesian methods, used to define the geo-electrical structure of the near-surface soil. These algorithms have demonstrated their usefulness in mapping the clay content of the Bt horizon associated with the control of encroaching trees.

© 2013 Elsevier B.V. All rights reserved.

1. Introduction

Slingram methods are based on electromagnetic induction, and are widely used to characterize upper soil horizons, taking advantage of the fact that different layers of soil can be characterized (and mapped) as a function of measured variations in electrical conductivity. Among the various commercially available devices, the EM38 and the new EM38-MK2 from Geonics operate at scales that are well suited to typical upper soil layers (Corwin and Lesch, 2005). The generalized use of the Slingram method, which has been well documented (McNeill, 1980), is very popular because it can be rapidly applied in the field (no galvanic contact required), and can be used for several environmental purposes as well as other methods providing the electrical conductivity (EC). The EC determined from such geophysical surveys is a significant characteristic, and depends on soil parameters of interest to soil scientists and environmentalists. The Slingram method has also been used to assess soil salinity processes (Lesch et al., 1995; McNeill, 1992; Rhoades et al., 1989; Williams and Baker, 1982), for precision agriculture (Kitchen et al., 2005; Lund et al., 1999; Mueller et al., 2003; Sudduth et al., 2001), for geomorphological and sedimentation purposes (Kitchen et al., 1996; Saey et al., 2008), and has been shown to be useful for the characterization of soil water content (Brevik et al., 2006; Hanson and Kaita, 1997; Hezarjaribi and Sourell, 2007; Kachanoski et al., 1990; Khakural et al., 1998; Sherlock and McDonnell, 2003) and/or clay content (Cockx et al., 2007; Doolittle et al., 1994; Kitchen et al., 1999). The Slingram method has also been used in the study of interactions between plants and soils, through measurements of the bulk soil EC (Hossain et al., 2010; Myers et al., 2007).

Depending on the user's requirements, the data can be interpreted in a qualitative mode, for example to delineate specific zones (salty or clayey areas) or in a quantitative mode, in which physical parameters need to be determined. Such applications involve the measurement of the conductivity of a given layer (or area), which is then converted into hydrological parameters (water or clay content), and measurements of the soil's geometrical organization, in particular the thickness of the upper layers. In the qualitative mode, field operation is rapid and

* Corresponding author at: Consulate General of France, The Lenox Building, 3399 Peachtree Rd NE, Ste 500, Atlanta, GA 30326, USA. Tel.: +1 33 622374714.
E-mail address: nicolas.florsch@upmc.fr (N. Florsch).

0016-7061/$ – see front matter © 2013 Elsevier B.V. All rights reserved.
http://dx.doi.org/10.1016/j.geoderma.2013.01.020

does not involve accurate conductivity determinations. In the quantitative mode, care must be taken with the field procedure and data post-processing, due to the main drawback of the Slingram method, i.e. its sensitivity to drift, which generally perturbs the measurements.

Drift effects depend on built-in features inherent to the apparatus, and arise from the difficulty in separating the secondary and primary electromagnetic fields. The secondary field, generated within the ground, is proportional to the ground's conductivity. However, the receiving coil also intercepts flux from the primary field, which is much stronger than that resulting from secondary field induced in the ground. This primary field is compensated electronically, but is prone to electronic drifts due to the temperature sensitivity of the in-built semi-conductors, a steady decrease in the battery voltage, and deformations of the device's housing (also of thermal origin). Robinson et al. (2004) provided an analysis of the origin and features of the EM38 drift, and Sudduth et al. (2001) proposed a procedure to reduce its effects, in a paper devoted to precision agriculture.

The drift in the measurements results from variations in the applied primary field compensation, and is an additive effect, although it is not directly proportional to the magnitude of the signal. It can be nulled through the use of rather delicate adjustments in the separation between the in-phase and quadrature signals made by the operator at the very beginning of the survey. The drift tends to be strong just after the device has been turned on, and several minutes should be allowed for thermal stabilization of the electronics, prior to data acquisition. Thereafter, the most sensitive effect is that arising from direct exposure of the device to the sun, such that it is desirable to maintain constant exposure to the sun, rather than vary the orientation of the stand. Working during cloudy conditions can be advantageous.

From our experience, the maximum drift observed with the EM38 was several tens of mS/m within a period of 1 h. For the EM38-MK2, the drift has been considerably reduced, to 1 or 2 mS/m for the same duration, in the 1 m spacing configuration. The 50 cm spacing behaves like the 1 m spacing of the older device. A special procedure, which can be used to prevent such drift effects, is discussed later in this paper.

The Slingram device integrates the ground conductivity of a given volume below the instrument, as described by McNeill in his seminal paper (1980). This method can be used to target 3-D structures, as in mining, or to characterize the geo-electrical parameters of a layered medium, in particular the upper soil horizons.

In the present paper we make use of the second type of application only, and are concerned only by variations in the 1-D conductivity as a function of depth, in profiles no deeper than those which can be investigated with the EM38, i.e. approximately 2 m. It is assumed that not more than three homogeneous layers could be realistically resolved. Our aim was to process the Slingram conductivity measurements, using a Bayesian methodology to invert the EM38 data in order to retrieve the thickness and conductivity of the topsoil, and the conductivity of the subsoil. In a second step, these conductivities can be converted into clay content values.

2. The EM38: basic characteristics, field procedure, and accurate drift correction

2.1. Basics

The EM38 has a 1 m spacing between the transmitter and receiver coils, whereas the EM38-MK2 has three coils (1 transmitter and two receivers), corresponding to two inter-coil spacings: 1 m and 50 cm. Geonics also markets devices with other spacings: 2 m (EM31-SH), 3.66 m (EM31), 10, 20 and 40 m (EM34). Other manufacturers such as DUAMLEM propose equivalent systems (see for instance Saey et al., 2009), which are also used for shallow investigations. Abdu et al. (2007) have compared the EM38 and the DUALEM-1S. GSS also produces the "Profiler EMP-400" with a 1.25 m spacing.

The Technical Note written by McNeill (1980) describes, in particular, the response of the apparatus in the presence of a layered medium. In most of the present paper, we consider the case of a soil structure with two horizontal (parallel to the surface) layers, of which the upper layer has a conductivity σ_1 and thickness h, and the second layer has a conductivity σ_2. In the VDM (Vertical Dipole Mode), the apparent conductivity (when the device is lying on the ground) is given by:

$$\sigma_a^V = \sigma_1[1-R_V(z)] + \sigma_2 R_V(z) \quad \text{with} \quad R_V(z) = \frac{1}{\sqrt{4z^2+1}} \quad \text{where} \quad z = h/s; \tag{1}$$

where s is the inter-coil spacing.

In the HDM (Horizontal Dipole Mode), we have:

$$\sigma_a^H = \sigma_1[1-R_H(z)] + \sigma_2 R_H(z) \quad \text{with} \quad R_H(z) = \sqrt{4z^2+1} - 2z. \tag{2}$$

In general, the VDM and HDM modes are used together. This "data pair" can also be obtained through the use of two different instruments, as described by Sudduth et al. (2010), who combined the EM38 from GEONICS, and the DUALEM-2S from DUALEM, to characterize an argillic horizon.

An alternative field procedure consists in maintaining the apparatus at a given height Z above the ground, to provide an additional measurement: the apparent conductivity is then determined according to a different integral of conductivity as a function of depth: the weighting of the shallow depths (topsoil) is decreased, whereas the contribution from the greater depths (subsoil) is increased, such that the apparent conductivity for the vertical mode is given by:

$$\sigma_a^Z = \sigma_1\left[R_V\left(\frac{Z}{s}\right) - R_V\left(\frac{h+Z}{s}\right)\right] + \sigma_2 R_V\left(\frac{h+Z}{s}\right). \tag{3}$$

The same relationship can be applied to the horizontal mode by substituting R_v into R_H.

More generally, EM induction "soundings" can be performed with the Slingram technique using two different methods:

- method 1: by increasing the coil spacing; in the case of the GEONICS instruments, one could combine two or more of the following devices: EM38-MK2, EM31-SH, EM31, EM34, leading to the following spacings: 0.5 m, 1 m, 2 m, 3.66 m, 10 m, 20 m, and 40 m. The use of both vertical and horizontal modes then allows a total of 14 independent values to be measured. As an example, this approach was used by Triantafilis and Monteiro Santos (2009), by combining the EM38 and EM34 systems, and by the same authors in 2010 with an EM38 coupled with an EM31. The VDM–HDM data pair can be substituted in the same manner, to analyze the soil at two different depths through the use of two different instruments. This approach was used by Sudduth et al. (2010), who combined an EM38 from GEONICS with a DUALEM-2S, to characterize an argillic horizon.
- method 2: by increasing the height of a single instrument above the ground, as described by Hossain et al., 2010. When the instrument is positioned at a greater height above the ground, although the depth of investigation is increased, the S/N ratio is degraded due to the increased separation between the soil and the coils.

2.2. Calibration: note on the classical scheme

The EM38 requires two main calibration procedures. The first of these is devoted to the in-phase component (providing a signal that depends on the susceptibility, not discussed here), whereas the second procedure, described in the following, compensates for the phase error.

This second procedure concerns the quadrature-phase signal, and consists in canceling the drift value at one point. However, following this adjustment the drift may reach a level of several mS/m after a

period of a few minutes or tens of minutes. It is thus essential that it be taken into account and corrected for during the survey.

The standard calibration scheme is based on the following method, and is related to the first procedure by the theory for the response of a thin conductive layer at a distance z below the instrument. This case leads to a pair of VDM–HDM responses having the ratio:

$$\frac{\Phi_V}{\Phi_H} = \frac{2z}{(4z^2+1)^{3/2} - 2z(4z^2+1)} = \varphi(z). \quad (4)$$

The ratio $\varphi(z)$ tends to 2 when z increases, and has a light discrepancy (with respect to 2) of 7% when $z = 1.5$ (cf. Figure 1). This is the basis of the calibration method (designed to null the offset drift), as proposed by GEONICS in the EM38 manual: the ratio is adjusted to 2 when the apparatus is held 1.5 m above the ground (let us call this "the factor 2 principle"). The 7% error is considered to be sufficiently accurate, since it relates to a pair of measurements obtained relatively high above the ground: the absolute error is less than 1 mS/m if the conductivity observed at this height is less than 14 mS/m (7% of 14 mS/m = 1 mS/m). This would be the apparent conductivity observed at this height, if the half-space had a homogeneous conductivity of 44 mS/m. In other words, this calibration procedure is accurate to the level of $1/44 \simeq 2\%$. The accuracy is in general even better than 2%, since not only the topsoil, but also the deeper layers of soil contribute (even more strongly, since they are integrated) to the measured signal. It should also be noted that natural heterogeneities of the soil would make a higher accuracy requirement unnecessary. In practice, as these devices are more often used for qualitative featuring than for accurate inversion applications, their accuracy following calibration is rarely mentioned in the literature.

With the EM38-MK2, a 50 cm coil spacing is used and this device can be considered to be equivalent to two instruments (using a common transmitter coil), such that the calibration must be made separately for both spacings. Although the equivalent height required for the calibration is 1.5 m/2 = 75 cm, a height of 1.5 m produces even better results than for the 1 m spacing and can be used at the same time as the 1 m spacing.

2.3. Field procedure and accurate drift correction

With the modern EM38, data can be recorded using an "auto" walking mode, in which conductivity measurements are collected at a rate of several readings per second. However, this introduces disturbances and fluctuations in the data (for example as a consequence of small variations in the height of the device above the ground) and should be avoided if it is planned to invert the data. With the help of a suitable positioning system, measurements can then be made over a regular grid or any other type of profile. As described in the following, in the present study we used a regular grid formed by an assembly of parallel lines separated by 5 meter spacings. Data was recording along each line (at points conventionally referred to as 'stations' in geophysics), using the same 5 m sampling interval. The x-axis of the map matches the line number, and the successive stations are positioned along the y-axis. The profiles are recorded parallel to the lines (y-axis) and are 50 m long.

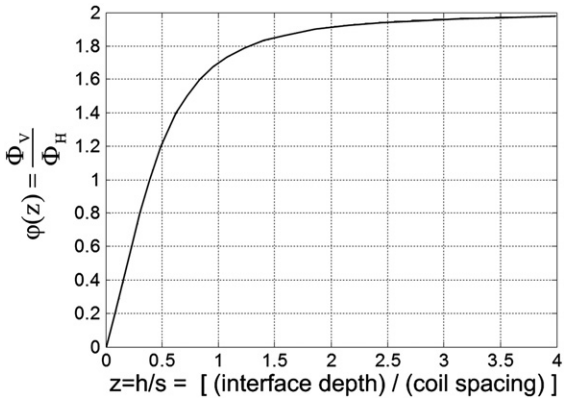

Fig. 1. The ratio $\varphi(z) = \frac{\Phi_V}{\Phi_H}$ versus the normalized height of the instrument. The calibration assumes that a factor two is reached. Actually, by holding the EM38 1.5 m above the ground, a resolution of 1 mS/m can be achieved (see the detailed discussion in the text).

When an accuracy better than 1 or 2 mS/m is needed, the most challenging requirement is that of correctly managing drifts in the instrument's sensitivity. Although these effects are greatly reduced in the recent EM38-MK2, when it is operated with a 1-m coil spacing, they are still significant when a 0.5 m inter-coil distance is used. Although the instrumental drift is not a major issue in the case of high soil conductivities or in the frame of semi-quantitative observations (e.g. when used to map relative salinity), it becomes a critical disturbance when the conductivities are low, because its magnitude approaches the observed conductivity. This occurs frequently when the conductivity is less than 10 mS/m, making it impossible to accurately invert the data.

Several strategies can be used to reduce the effects of drift:

- Post-filtering of the data, forcing it to match an expected statistical profile (assuming for example that the mean values of the different profiles should all be equal). This procedure can produce satisfactory results, but does not take the absolute value of the drift into account;
- Renewal of the calibration procedures whenever possible (for instance for each profile). This is effective only for a short period of time following each calibration operation;
- Analysis of cross-over profile discrepancies, starting at the beginning of the survey;
- Use of regular drift measurements and interpolation, in order to correct for the drift at any moment during the observations. This method is also used in gravity and magnetic (for instrumental and/or natural time-depending variations).

The latter strategy was considered to be the most accurate. In the following, we provide a detailed description of its practical implementation, based on the theory of the instrument.

2.3.1. Efficient management of drift

It is in all cases appropriate to calibrate the instrument at the very beginning of the survey. In order to estimate the drift at any given time, one possible method requires measurements to be made at regular intervals in time, at the same location. The recorded data can then be interpolated as required. This first method is very time consuming on the field, as it requires the operator to return to the same location at regular intervals (typically every 15 min).

We tested a second method, which was found to be considerably more efficient: it consists in calculating the drift at any location, by using the "factor 2 principle" at a height of 1.5 m. This method begins with a drift calculation, using the calibration procedure provided by GEONICS for the EM38, but goes a step further in the use of this calculation.

If it is first considered that the instrument has drifted, then:

$$\frac{\sigma_V^a(1.5)}{\sigma_H^a(1.5)} \neq 2 \quad (5)$$

at a height of 1.5 m (although this value is not repeated hereafter, it remains implicit in the following).

The offset C which must be applied to the readings, in order to obtain a factor of exactly 2, is obtained by solving the equation:

$$\frac{\sigma_V^a + C}{\sigma_H^a + C} = 2 \quad (6)$$

from which:

$$C = \sigma_V^a - 2\sigma_H^a. \quad (7)$$

The drift is simply:

$$D = -C = 2\sigma_H^a - \sigma_V^a. \quad (8)$$

Then the drift can be corrected for by subtracting D from the readings without adjusting the device potentiometers: this provide a final measure cleaned from the drift.

We thus applied the following algorithm to correct for drift, during the course of a set of soil conductivity measurements:

- First make an initial calibration (possibly not perfect)
- Make the 1st drift measurement: instrument 1.5 m above the ground, "where you are"
- Make a set of measurements (5 to 20?)
- Make the 2nd drift measurement, "where you are"
- Make a set of measurements
- Make the 3rd drift measurement, "where you are"
- …
- …
- Make the last drift measurement, "where you are".

No re-calibration (adjustment of potentiometers) is required in the field, and the data is post-processed by applying suitably interpolated drift corrections.

In the results presented here, we were able to achieve an accuracy ranging between 1 and 2 mS/m, by measuring the drift at every 22nd station. The results would have been slightly more accurate if the drift measurements had been made at 5 or 10 station intervals.

3. Field procedure and non Bayesian inversion of the data: a brief review

As the Slingram method can be implemented rapidly in the field, it is often used to map the conductivity on a 2-D grid. At each field point, the device can be used to record several measurements, depending on the available coil spacing and the attitude of the device.

The EM38 (with its one meter coil spacing) and the EM38-MK2 (with two coil spacings: 50 cm and 1 m) allow various measurement procedures to be used. The simplest of these consists in measuring the VDM only, with a single spacing. A more complex approach involves a set of measurements made in both modes (VDM and HDM), with two different coil spacings. Moreover, it is possible to perform additional measurements by raising the device to a height typically 50 cm above the ground. The data thus obtained has a greater sensitivity to deeper components of the subsoil, because the weighting of the latter is increased with respect to that of the shallower layers (even though the total signal is reduced as a result of the increase in separation between the instrument and the conductive soil). Physically speaking, these different measurements are composed of differently weighted integrals of the ground resistivities. Hence, the greater the number of different measurements, the greater the number of independent parameters that can be inverted.

In the following, we first discuss possible approaches to the inversion of Slingram data using non-Bayesian methods. In particular, we evaluate the feasibility of finding an analytical solution in some cases.

Slingram data inversion may correspond to several different cases:

1) The data is not inverted, and only raw conductivity maps are proposed. This is typically the case when only one type of data is collected (VDM, 1 m coil spacing, for instance).
2) The data is not inverted using a physical law, but some correlations are established between the apparent conductivity and the soil parameter of interest, then permitting to convert the data into soil parameters. Using this approach, Domsch and Giebel (2004) converted the apparent conductivity directly into soil texture through the use of established correlations. One or more measurements may be used. Although such methods are certainly robust, the role of some "laws of equivalence" and parameter correlations could be missed. When data inversion is performed, the number of data points is less than the number of model parameters; this is the so-called "underdetermined case" (Menke, 1989), in which some a priori information is needed in order to perform the inversion. Within the EM38 community, this a priori information often takes the form of a Thikonov regularization, which consists in including a certain level of model smoothness, controlled by the "damping parameter". When expressed in terms of an a priori covariance matrix, it is equivalent to a diagonally dominant weighting. This corresponds to the approach proposed by Deidda et al. (2003) and Hendrickx et al. (2002). The case in which a multi-layer model (including numerous parameters) is inverted from a small quantity of EM38 data is a canonical example of such an underdetermined problem.
3) Inversion with the quantity of data being equal to the number of parameters (for instance two conductivities and one thickness to be retrieved from 3 apparent conductivities). This corresponds to the "even-determined case". Here, an analytical inversion is theoretically possible. However, it can be shown that this is feasible only under certain conditions. We briefly discuss this possibility in the following.
4) Proper inversion where the quantity of data is greater than the number of parameters to be recovered: this is referred to as the "overdetermined case". A least-squares (LSQ) method (with or without damping) is the most common approach to the management of such a case.

It should be noted that a very general frame theory "containing" all such inversion methods is provided by the Bayesian approach, as shown by Tarantola and Valette (1982a, 1982b).

In the present paper, we deal only with the simple, two-homogeneous-layer model. This simplified model has a topsoil of conductivity σ_1 and thickness h, and a subsoil of conductivity σ_2 down to the limit of the investigation depth of the EM38 (approximately 2 m in practice). The three unknown parameters are thus: σ_1, σ_2 and h.

3.1. The analytical approach

For a case corresponding to point 3, it is tempting to use an analytical approach, because three measurements should be sufficient to recover the three unknown parameters $\{\sigma_1, \sigma_2, h\}$. With a classical EM38, the 3 measurements could be provided by the two modes on the ground (VDM and HDM), together with a VDM measurement, with the instrument being held at a given height above the surface (Z = 50 cm in our case), in order to record additional data from a greater depth. Such a dataset leads to a system of three equations with three unknowns, where σ_a^V and σ_a^H are the VDM and HDM data respectively (with the apparatus on the ground), and σ_a^Z is the apparent conductivity when the device is held vertically at a height Z above the ground.

$$\begin{cases} \sigma_a^V = \sigma_1[1-R_V(h)] + \sigma_2 R_V(h) = \sigma_1[1-R_V] + \sigma_2 R_V \\ \sigma_a^H = \sigma_1[1-R_H(h)] + \sigma_2 R_H(h) = \sigma_1[1-R_H] + \sigma_2 R_H \\ \sigma_a^Z = \sigma_1[R_V(Z)-R_V(Z+h)] + \sigma_2 R_V(Z+h) = \sigma_1\left[R_V^0 - R_V^h\right] + \sigma_2 R_V^h \end{cases} \quad (9)$$

The third expression given in each line results from a simplification of the notation.

With the EM38-MK2 device, although it is natural to consider both modes with the 1 m spacing, we propose using the vertical mode with the 50 cm spacing. As the horizontal mode has a very superficial response, and it is difficult to position the apparatus on the ground

with a truly horizontal orientation (especially in the presence of grass or slight undulations), this is the noisiest of the various types of measurement that can be made. It is thus generally preferable to avoid such an observation, and to keep only three values for analytical inversion. It should be noted that the direct calculation can be improved by including a thin layer of air that would take the effective height of the center of the coil (which varies depending on whether the vertical or horizontal mode is used) into account.

In this case, the system is: (the ~ will hold for the 50 cm spacing).

$$\begin{cases} \sigma_a^V = \sigma_1[1-R_V] + \sigma_2 R_V \\ \sigma_a^H = \sigma_1[1-R_H] + \sigma_2 R_H \\ \sigma_a^{\tilde{V}} = \sigma_1[1-R_{\tilde{V}}] + \sigma_2 R_{\tilde{V}} \quad \text{where} \quad R_{\tilde{V}} = \dfrac{1}{\sqrt{4\left(\dfrac{h}{0.5}\right)^2+1}} = \dfrac{1}{\sqrt{16h^2+1}}. \end{cases} \tag{10}$$

Mathematically speaking, theses two systems can be solved as long as the number of observations is exactly equal to the number of parameters. When solved linearly, by firstly eliminating σ_1 and σ_2, this leads to a single equation $f(h)=0$, which can be solved numerically (or even analytically). However, such an ideal situation rarely occurs in practice, and it is common that no real solution can be found. This is because the data is strongly affected by errors, such that the system to be solved (for example that described above for two kinds of EM38) may have no solution at all. This is due to the fact that the image space (E) of the application $\{\sigma_1,\sigma_2,h\}\mapsto\left\{\sigma_a^V,\sigma_a^H,\sigma_a^{\tilde{V}}\right\}$ is just a small part of $\Re^3$, and very often the resulting sets of noisy measurements do not correspond to any original model in the parameter space. Equivalently, the noise causes the data to exit the domain E. Consequently, the LSQ method, a Bayesian inversion, or any other method which does not require the solution to exactly match the measurements, is required in order to overcome this difficulty.

3.2. Positivity constraint

When an inversion technique is applied to EM38 data, a positivity constraint must be applied to the conductivities and the thicknesses of the layered model. Otherwise, most of the algorithms can be unstable in the sense that spurious solutions may arise. The best way to meet this requirement is to use the logarithm of the parameters, instead of the parameters themselves. This approach also ensures that all of the parameters are Jeffrey's parameters (see Jeffrey's, 1939 book, and also Tarantola, 2005, 2006).

3.3. Other inversion perspectives

Until now, little attention has been paid in the literature to less conventional techniques. However, methods such as the Particle Swarm Optimization (PSO), see for example Trelea (2003) and Fernández-Martínez et al. (2011), the Simulated Annealing method (Kirkpatrick et al., 1983), and certainly the homotopy method, described by Jegen et al. (2001), which was used by Ghorbani et al. (2009) to invert induced polarization data, can also lead to a satisfactory inversion of the data.

4. Bayesian methods

4.1. Principle of the method

The Bayesian approach consists in working with the Probability Density Functions (PDF), or simply "Probability Measures" (PM) when the probability laws cannot be normalized. Through the Bayesian theorem, the Bayesian method combines, collects and correlates knowledge of the system (the a priori knowledge) before any measurements are made, and the new emergent knowledge provided by the measurement campaigns. The a priori information includes not only whatever insight the user has of the system parameters, but also the choice of the model itself. The two-layer model we use here is thus a component of the a priori knowledge (although this a priori knowledge is not normally expressed in numerical form).

The Bayesian method has been widely discussed, since it was summarized by Tarantola and Valette (1982b), and described in greater detail by Tarantola (2005). Currently, the use of Bayesian methods remains slightly controversial, with a (formal?) opposition existing between the so-called "frequentists" and the Bayes defenders. Carlin and Louis (1998) wrote an excellent book on the Bayesian approach, whereas Scales and Sneider (1997) discussed this type of approach from the philosophical/Shakespearian point of view.

In the present study we use an implementation very similar to that used by Ghorbani et al. (2007), and by Florsch and Hinderer (2000), who provide a detailed description of all of the required concepts. Some of these are mentioned only briefly in the following.

Let $\vec{d}$ be the data, $\vec{m}$ the model and $\vec{d}=G\left(\vec{m}\right)$ the physical law relating these quantities. In the case of an overdetermined inversion, $\dim\left(\vec{m}\right)<\dim\left(\vec{d}\right)$.

Let $\mu\left(\vec{m}\right)$ be the "homogeneous probability measure" (see Tarantola, 2005). It should be noted that if $\vec{m}=(m_1,m_2,\ldots m_{\dim(M)})$, these are all Jeffrey's parameters, and we have

$$\mu\left(\vec{m}\right)=\frac{1}{m_1}\frac{1}{m_2}\ldots\frac{1}{m_M}, \tag{11}$$

(this is the case since the conductivities and thicknesses are Jeffrey's parameters).

Since we generally apply logarithmic transformations to all Jeffrey's parameters, it can be shown that

$$\mu(\log(m_k))=\text{const.},\ \forall k. \tag{12}$$

This simplifies the computation, since these terms can be dropped (for the purposes of the calculations only).

In our model, all parameters of the Jeffrey's type, that is the "homogeneous probability measure" (previously referred to as "null information" in the work of Tarantola) are:

$$\left\{\mu_1(\sigma_1)=\frac{C_1}{\sigma_1};\ \ \mu_2(\sigma_2)=\frac{C_2}{\sigma_2};\ \ \mu_3(h)=\frac{C_3}{h}.\right. \tag{13}$$

One feature of these probability measures is that they cannot be normalized. In practice, they are always involved in a more complex expression of the PDF that can be normalized at the end of the process. Note that those probability measures can be derived from the modern Shannon definition of informational entropy (see Tarantola and Valette, 1982a).

As we systematically use the parameters' logarithms (see for instance Florsch and Hinderer, 2000 or Ghorbani et al., 2007 for additional arguments), the following changes are made:

$$\sigma_1^{\log}=\log(\sigma_1);\ \ \sigma_2^{\log}=\log(\sigma_2);\ \ h^{\log}=\log(h). \tag{14}$$

This accommodates the fact that all of these parameters are Jeffrey-like. As a matter of convenience, the logarithm is taken in base 10.

We note $\phi\left(\vec{m}\right)$ for the a priori PDF of the parameters. Logically speaking, this PDF does not contain the full a priori knowledge, but only the quantitative part of it. The density ϕ could be Gaussian, or any other distribution. It is frequent to use the combination (product) of a Gaussian PDF, with the indicator function of the interval to be

explored, in order to find the parameters (that is, a windowed exploration box).

Let us assume, for example, the following a priori information:

"σ_1^{log} could be close to 0.5 ± 0.3"

(this must be translated into: σ_1^{log} follows a Gaussian distribution of mean value 0.5 and standard deviation 0.3, that is σ_1 is assumed to be close to 3.13, with a 30% error), and we determine its value between 0 and 1 only. The a priori PDF should then be:

$$\phi\left(\sigma_1^{log}\right) = C \cdot I(0,1) \cdot e^{-\frac{1}{2}\left(\frac{\sigma_1^{log}-0.5}{0.3}\right)^2}, \tag{15}$$

where C is a normalization constant and I (0,1) is the index function equal to 1 in the interval [0, 1] and 0 outside this interval. The same applies to the other parameters and the full 3-variables a priori is just the product of the three similar probability distributions.

We also assume that the data follows a Gaussian PDF, with a covariance matrix C_{dd}. The PDF of the parameters, which is also *the* solution of the inverse problem, is then given by:

$$pdf\left(\vec{m}\right) = \frac{\phi\left(\vec{m}\right) e^{-\frac{1}{2}\left[\vec{d}-G\left(\vec{m}\right)\right]^T C_{dd}^{-1}\left[\vec{d}-G\left(\vec{m}\right)\right]}}{\mu\left(\vec{m}\right)}. \tag{16}$$

This is the quantity we compute and plot in a Bayesian inversion. In the present case, thanks to the logarithmic change of variable, the homogeneous probability measure can be dropped (because it becomes constant), and this PDF can be computed directly by means of a systematic exploration over a regular (3 dimensional) grid. This is achieved by scanning the parameters within pre-defined intervals.

The computation can thus be fully developed, using the following steps:

1) Define, for example, exploratory intervals and grids for σ_1^{log}, σ_2^{log} and h^{log},
   Grid for σ_1^{log}: defined from $\sigma_{1\,min}^{log}$ to $\sigma_{1\,max}^{log}$ at N_{σ_1} regularly spaced points. Apply the same procedure to the other parameters, leading to the final index function:

$$I\left(\left[\sigma_{1\,min}^{log}, \sigma_{1\,max}^{log}\right]; \left[\sigma_{2\,min}^{log}, \sigma_{2\,max}^{log}\right]; \left[h_{min}^{log}, h_{max}^{log}\right]\right). \tag{17}$$

   In practical terms, this implies that the parameter space is explored only within this 3-D box, over $N_{\sigma_1} \times N_{\sigma_2} \times N_h$ points.
2) Define (or not) an (a priori) Gaussian (or other) law for the parameters distribution. As an example, in the following it is assumed that a Gaussian law can be used to describe σ_1^{log} and h^{log} (assumed to be independent), and that no additional law is needed for σ_2^{log} (i.e. the law is uniform for the relevant interval):

$$A\left(\sigma_1^{log}, \sigma_2^{log}, h\right) = \exp\left[-\frac{1}{2}\left(\left(\frac{\sigma_1^{log}-\overline{\sigma}_1^{log}}{\delta\sigma_1^{log}}\right)^2 + \left(\frac{h^{log}-\overline{h}^{log}}{\delta h^{log}}\right)^2\right)\right], \tag{18}$$

   where $\delta\sigma_1^{log}$ represents the standard error on the parameter σ_1^{log} and $\overline{\sigma}_1$ log represents the most probable or mean value of σ_1^{log} (and the same for h respectively). We do not use a normalization factor in the expression for the PDF, because normalization can be performed at the end of the process. This leads to our definition for the a priori PDF, which can be written: $\phi = I \cdot A$. In practice, an additional law such as that given in expression (18) is not always required, but can be very useful in avoiding the equivalence problem, as discussed below. Notice that we choose to put a priori on sigma1 because it is difficult to assess as it is of the same order of magnitude than the accuracy itself. We choose to set an a priori on h because it can be derived from the field pits and also to limit the equivalence consequence on the whole inversion.
3) When it can be assumed that the data are independent and have a Gaussian distribution, the law describing the experimental results is (with 'th' is for theoretical and 'obs' for observed):

$$D\left(\sigma_1^{log}, \sigma_2^{log}, h\right) = \exp\left[-\frac{1}{2}\left(\left(\frac{\sigma_a^{Vth}-\sigma_a^{Vobs}}{err\left(\sigma_a^{Vobs}\right)}\right)^2 + \left(\frac{\sigma_a^{Hth}-\sigma_a^{Hobs}}{err\left(\sigma_a^{Hobs}\right)}\right)^2 + \left(\frac{\sigma_a^{Zth}-\sigma_a^{Zobs}}{err\left(\sigma_a^{Zobs}\right)}\right)^2\right)\right], \tag{19}$$

   this is also the case when an additional measurement has been included, for example by holding the apparatus at a height Z above the ground, or:

$$D\left(\sigma_1^{log}, \sigma_2^{log}, h\right) = \exp\left[-\frac{1}{2}\left(\left(\frac{\sigma_a^{Vth}-\sigma_a^{Vobs}}{err\left(\sigma_a^{Vobs}\right)}\right)^2 + \left(\frac{\sigma_a^{Hth}-\sigma_a^{Vobs}}{err\left(\sigma_a^{Hobs}\right)}\right)^2 + \left(\frac{\sigma_a^{\tilde{V}th}-\sigma_a^{\tilde{V}obs}}{err\left(\sigma_a^{\tilde{V}obs}\right)}\right)^2 + \left(\frac{\sigma_a^{\tilde{H}th}-\sigma_a^{\tilde{V}obs}}{err\left(\sigma_a^{\tilde{H}obs}\right)}\right)^2\right)\right]. \tag{20}$$

   This would apply, for instance, if measurements had been made with the EM38-MK2, using both 1 m and 50 cm coil separations (noted by ~).
   Finally, the function to be estimated is the 3-D PDF:

$$P\left(\sigma_1^{log}, \sigma_2^{log}, h\right) = I\left(\sigma_1^{log}, \sigma_2^{log}, h\right) \cdot A\left(\sigma_1^{log}, \sigma_2^{log}, h\right) \cdot D\left(\sigma_1^{log}, \sigma_2^{log}, h\right). \tag{21}$$

   In this expression, even the homogeneous probability measure is taken into account, because $P\left(\sigma_1^{log}, \sigma_2^{log}, h\right)$ is computed over a logarithmically defined grid, with sampling of the logarithm of the variables being made at regular intervals. Once this distribution has been computed, the correctly normalized PDF can be written as:

$$p\left(\sigma_1^{log}, \sigma_2^{log}, h\right) = \frac{P\left(\sigma_1^{log}, \sigma_2^{log}, h\right)}{\iiint P\left(\sigma_1^{log}, \sigma_2^{log}, h\right) d\sigma_1^{log} d\sigma_2^{log} dh}. \tag{22}$$

   All of the integrals used in this paper involve functions which are known on grids, then simple Riemann summations can be used to estimate them.
   According to Tarantola and Valette (1982a), this function is the solution to the inverse problem: it allows the probability of a set of parameters belonging to a given interval to be calculated. This can be expressed as:

$$prob\left(\sigma_1^{log} \in \Gamma_{\sigma_1}, \sigma_2^{log} \in \Gamma_{\sigma_2}, h \in \Gamma_h\right) = \int_{\Gamma_{\sigma_1}} \int_{\Gamma_{\sigma_2}} \int_{\Gamma_h} P\left(\sigma_1^{log}, \sigma_2^{log}, h\right) d\sigma_1^{log} d\sigma_2^{log} dh. \tag{23}$$

   At this stage, it is also important to evaluate the potential CPU/memory requirements for the evaluation of such functions. As expression (23) is 3-D function, a grid of say $100 \times 100 \times 100 = 10^6$ points would need to be managed by the computer. Although such a grid is moderate in size, it would rapidly become impossible to evaluate the above function for grids exceeding 100 points in each dimension. This restriction then leads to the following two questions: firstly, is the domain of exploration sufficiently

large (will it contain the solution?), and secondly, is the grid sampled at sufficiently close intervals to provide an adequate representation of the PDF? There is a risk of aliasing or even missing the main features of the law, if the grid is too coarse with respect to the function extent. In the case when problems of a higher number of dimensions must be tackled, it is useful to use special integration algorithms such as the so-called "metropolitan" scheme (as described by Mosegaard and Tarantola, 1995).

4.2. Representation of the solution, numerical example and equivalence analysis

The obtained PDF $P\left(\sigma_1^{\log}, \sigma_2^{\log}, h\right)$ is a function of three variables, and can be represented by a 3-D plot, as shown in Fig. 2. Although this type of plot is useful for purely visual interpretations (see for instance Ghorbani et al., 2007), it is not practical for the evaluation of quantitative results. Moreover, in general, the geophysicist needs to provide a single value for each parameter, with its corresponding errors. If only a single value (and its associated error) is required, this means that a considerable proportion of the information provided by this full probabilistic solution is discarded.

It can thus be useful to plot the 2-D marginal laws and, by cascading, the 1-D marginal laws, and finally the mean values and attached standard deviations.

Here, the first step of the marginal probability calculation yields three laws, using two parameters:

$$\begin{cases} p_{\sigma_1^{\log}\sigma_2^{\log}}\left(\sigma_1^{\log}, \sigma_2^{\log}\right) = \int_{h_{\min}^{\log}}^{h_{\max}^{\log}} p\left(\sigma_1^{\log}, \sigma_2^{\log}, h\right) dh \\ p_{\sigma_1^{\log}h}\left(\sigma_1^{\log}, h\right) = \int_{\sigma_{2\min}^{\log}}^{\sigma_{2\max}^{\log}} p\left(\sigma_1^{\log}, \sigma_2^{\log}, h\right) d\sigma_2^{\log} \\ p_{h,\sigma_2^{\log}}\left(h, \sigma_2^{\log}\right) = \int_{\sigma_{1\min}^{\log}}^{\sigma_{1\min}^{\log}} p\left(\sigma_1^{\log}, \sigma_2^{\log}, h\right) d\sigma_1^{\log} \end{cases} . \quad (24)$$

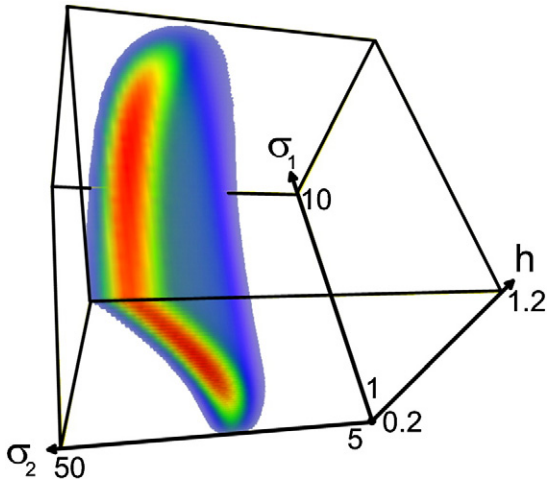

Fig. 2. 3D representation of the solution space obtained by Bayesian inversion. The original data corresponds to one corner point of our map: $\begin{cases} \sigma_a^{V(1m)} = 16.58 \pm 2 \\ \sigma_a^{H(1m)} = 10.17 \pm 2 \\ \sigma_a^{V(50cm)} = 9.86 \pm 3 \\ \sigma_a^{H(50cm)} = 6.17 \pm 4 \end{cases}$ mS/m. The red color pole shows the higher probability density function, while the parts let in blank is relative to a negligible probability density function.

The law for any one of the parameters is given by an integral of the form:

$$p_\alpha(\alpha) = \int p_{\alpha\beta}(\alpha, \beta) d\alpha\beta \quad (25)$$

for any pair of the above three expressions.

Finally, the mean and centered variance can be computed from the law, as:

$$\overline{\alpha} = \int \alpha p_\alpha(\alpha) d\alpha; \quad \mathrm{var}(\alpha) = \int (\alpha - \overline{\alpha})^2 p_\alpha(\alpha) d\alpha. \quad (26)$$

At this stage, it is straightforward to plot a map of the inverted parameters from apparent conductivity maps, and it can be expected that the above mean value will be close to the least-squares solution (at each map point).

Such a result is however very different from the least-squares solution, in terms of the quantity of information it provides. Indeed, the LSQ solution corresponds to the parameter set for which the maximum of the function D described above has been reached (the minimum of the exponent). The important difference is that a parameter retrieved from this LSQ solution does not involve any integration over the other parameters. In the case of Gaussian laws, and more generally symmetric PDFs, it makes no difference, because those integrals are centered on the mean value (even if the physical law involved is nonlinear). In all other cases, the marginal Bayesian solution is preferable to the LSQ solution, because it correctly integrates all possible cases.

The Bayesian solution is an interpretation which preserves information, and provides probabilities with which the parameters can be characterized. Furthermore, it facilitates the analysis of the equivalence laws by plotting the trade-off between parameters.

4.2.1. Analysis of the equivalence problem

To analyze the equivalence problem in the present case, we first consider the following problem: let us assume the case of a conductive topsoil a few decimeters thick, and a very resistive subsoil (with negligible σ_2). The following equivalence law may then be written:

$$\sigma_1(1 - R_V(h)) \equiv \sigma_1'(1 - R_V(h')) = \text{const.} \quad (27)$$

That is, the pair $\{\sigma_1, h\}$ will lead to the same apparent conductivities as $\{\sigma_1', h'\}$, especially when $\sigma_1 \to \infty$ and $h \to 0$ (area of equivalence), whilst respecting the condition

$$\sigma_1(1 - R_V(h)) = \text{const.} \quad (28)$$

Within this "area of equivalence", this law becomes:

$$2\sigma_1 z^2 = \text{const.} \quad (29)$$

Conversely, a relatively resistive layer covering a deeper conductive layer will lead to the following equivalence law (with negligible σ_1):

$$\sigma_2 R_V(h) = \sigma_2' R_V(h') = \text{const.} \quad (30)$$

The area of equivalence is defined by $\sigma_2 \to \infty$ and $h \to \infty$, and within the equivalence area:

$$\frac{\sigma_2}{2z} = \text{const.} \quad (31)$$

These laws are shown in Fig. 3, in which they are generalized for any inter-coil spacing (with $z = h/s$).

In Fig. 2, the resistive/conductive case is clearly visible, and involves the three parameters. However, when there is not a high contrast between the first and second layers, an equivalence can be expected between two parameters; here, we consider the case corresponding to Eq. (31). Examples of the three 2-by-2 marginal probabilities

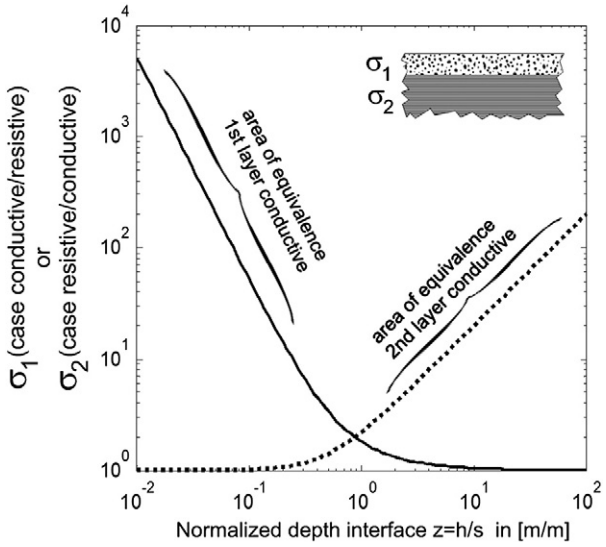

Fig. 3. Equivalence laws for a simple structure: conductive layer covering a resistive layer (Eq. (28)), or resistive layer covering a conductive layer (Eq. (30)).

are given in Fig. 4a, b, and c, and the final PDFs for the single parameters are shown in Fig. 4d, e, and f. In particular, the a priori information we use in this one-point study is:

$$\text{prior} = I(1 \le \sigma_1 \le 10) \cdot I(5 \le \sigma_2 \le 50) \cdot I(0.2 \le h \le 1.2). \quad (32)$$

It should be noted that the boundary limits can still affect the mean solution, with potentially dramatic consequences because, in mathematically terms, the average value includes the influence of distant values, i.e. corresponding to $\sigma_2 \to \infty$ and simultaneously $h \to \infty$ (compatible with the equivalence law). Such an outcome can be avoided by applying physical and geological knowledge, which in mathematical terms could be achieved by including a suitably shaped a priori law in the inversion process. This approach was used in the following.

The pattern in Fig. 4c shows that the predominant equivalence exists between the depth of the interface and the conductivity of the second layer, in agreement with the expected outcome.

When applying this method to a full geophysical map involving hundreds of data points, it is quite impossible to plot the full PDF, and only the mean values at the end of the queue process are shown. It is nevertheless possible to proceed at any time with an exploration of the full solution space in order to evaluate any desired points of interest.

It is now of interest to develop a methodology to prevent the equivalence law from having an influence on the solution, in particular the contribution of the distant components of the PDF when $\sigma_2 \to \infty$ and $h \to \infty$. This contribution, the significance of which depends on the width of the exploratory window, affects the mean values. The wider the window, the greater the bias added to the mean value. Mathematically speaking, this result could be expected, since this "remote" solution is still compatible with the data. However, as this bias leads to an unrealistic solution, it is desirable to remove or minimize its influence. A simple solution consists in introducing a form of a priori information which, for example, promotes low values of (h). This aspect of the data reduction is truly a matter of choice, and is thus

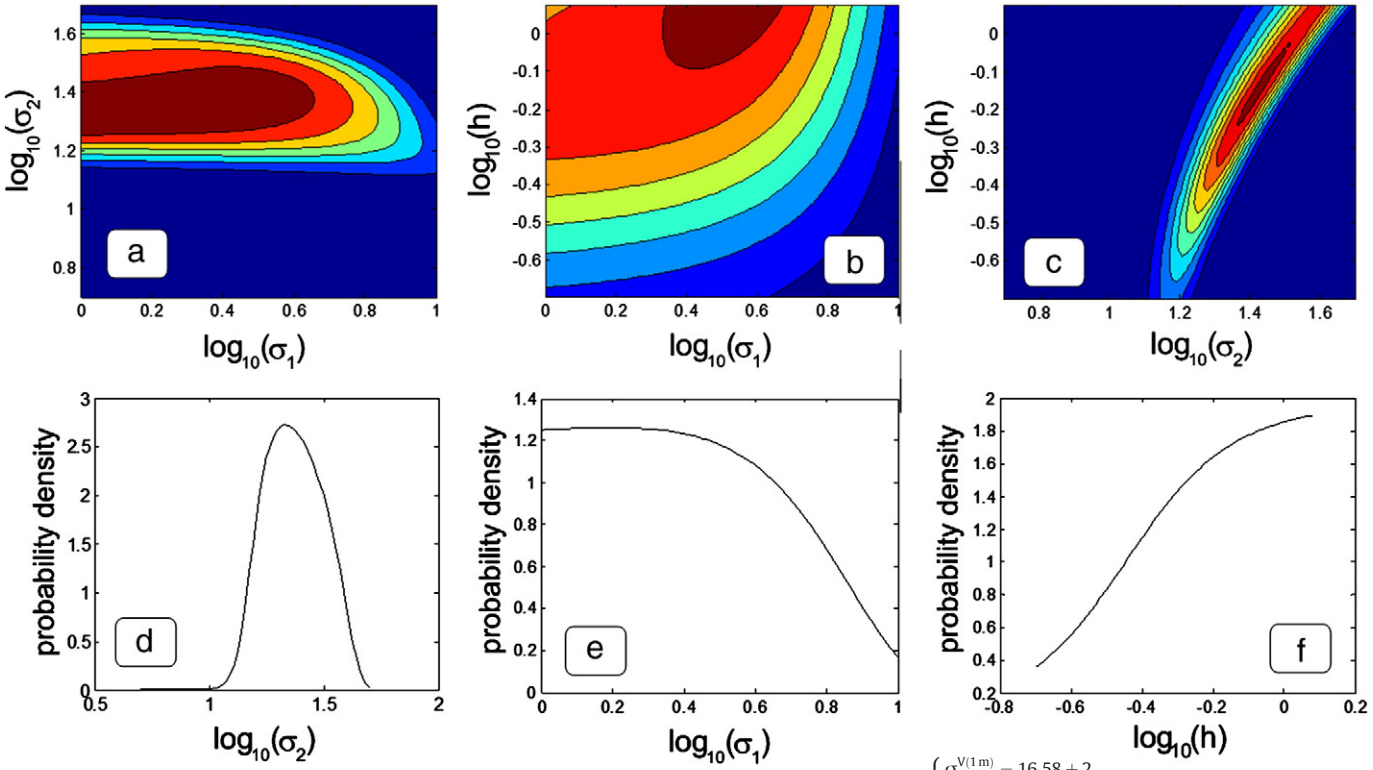

Fig. 4. Full marginal PDF after the Bayesian inversion of the same dataset than the one used to produce Fig. 2, that is: $\begin{cases} \sigma_a^{V(1\,m)} = 16.58 \pm 2 \\ \sigma_a^{H(1\,m)} = 10.17 \pm 2 \\ \sigma_a^{V(50\,cm)} = 9.86 \pm 3 \\ \sigma_a^{H(50\,cm)} = 6.17 \pm 4 \end{cases}$ mS/m. The 2D marginal probability density functions clearly reveal the predominant equivalences between (σ_2) and (h). Note that these images (for example case (c)) do not correspond to a particular slice of the solution space shown in Fig. 2, but to a projection onto a plane (for instance (σ_2, h)), which integrates the 3D function in the direction normal to this plane. The red color pole is relative to the higher probability density function, while the probability becomes negligible at the blue pole. The amplitude is relative but can be normalized by setting the integral to one to compute effective probabilities, once the exploration window set (the wider the exploration window, the lower the density).

a subjective component of the inversion. In the following, we adopt the a priori function:

$$\text{prior} = I(1 \le \sigma_1 \le 10) \cdot I(5 \le \sigma_2 \le 50) \cdot I(0.2 \le h \le 1.2) \cdot A(h) \quad (33)$$

where

$$A(h) = 1 - \frac{h}{1.2}, \quad (34)$$

which is simply a linearly decreasing function from 1 to 0 over the interval [0, 1.2] included in the exploration window [0.2 1.2]. Other decreasing functions could also have been chosen: this is the subjective aspect of the inversion process.

Fig. 5 illustrates the changes induced in this constrained case, with respect to Fig. 4. It illustrates the limiting effect, not only on (h), but also (as a consequence) on σ_2.

Fig. 5 also provides full knowledge of the resolution relative to each parameter. From Fig. 5a, b and e, it can be seen that the conductivity of the first layer is not well bounded at the lowest possible values. In practice, if this layer had been neglected (in terms of its conductivity, not its thickness) it would not have produced any change in the solution. This result is coherent with the level of noise we set (2 mS/m), with respect to the conductivity itself (less than 4 mS/m).

5. Example of an application at the Potshini site (KwaZulu-Natal, South Africa)

5.1. Context

Ecological studies have been undertaken at Potshini, in an effort to evaluate the phenomenon of tree encroachment (Grellier et al., 2012a, Grellier et al., 2012b). Tree encroachment in grasslands corresponds to an increase in the density, coverage and biomass of indigenous tree species (Van Auken, 2009). This phenomenon is recognized world-wide (Archer et al., 1995; Bond, 2008; Wiegand et al., 2005), and can have severe ecological consequences (Scholes and Archer, 1997; Smit, 2004) and economical repercussions (Burkinshaw and Bork, 2009), affecting 20% of the world's population (Turner et al., 1990). Soil properties can play a role in tree growth and the spatial distribution of trees (Schleicher et al., 2011). The upper sub-surface layers of soil (down to a depth of 2 m) are especially important, since most tree and grass roots co-exist (Schenk and Jackson, 2002). The Slingram method and Bayesian inversion methodology were applied in this context, in order to study the relationships established between various soil properties, in particular its clay content and the spatial distribution of grassland trees.

5.2. Site description

Our experiments were conducted at Potshini in a grassland area of KwaZulu-Natal, South Africa (28° 48′ 37″ S; 29° 21′ 19″ E, altitude 1300 m) (Figure 6), where tree encroachment began 25 years ago (Grellier et al., 2012b). The climate is sub-humid, sub-tropical, with a rainy summer (October–April) and a mean annual precipitation of 745 mm over the last 65 years. The mean annual temperature is 13 °C (Schulze, 1997) and potential evaporation is between 1600 mm and 2000 mm per year (Guy and Smith, 1995). The geology is represented by fine-grained sandstones, shales, siltstone and mudstones of the Beaufort and Ecca Groups, belonging to the Karoo Supergroup, which alternate in horizontal successions (King, 2002). Unconsolidated colluvial deposits from the Pleistocene continue to fill the valleys, and are very prone to gully erosion (Botha et al., 1994). The soils are classified into luvisols (World Reference Base 1998) with two well-delimited main horizons. The A-horizon is brown in color (10YR 4/1 to 10YR 4/3) and has a 20% clay composition (granulometric definition of clay: particle size less than 2 μm), but, with many fine and medium sized roots. The Bt Horizon (up to 50% granulometric clay) is dark brown in color, very coherent and hard, with a coarse blocky structure. Fig. 7 is a picture showing a gully wall, allowing identification of the topsoil A Horizon

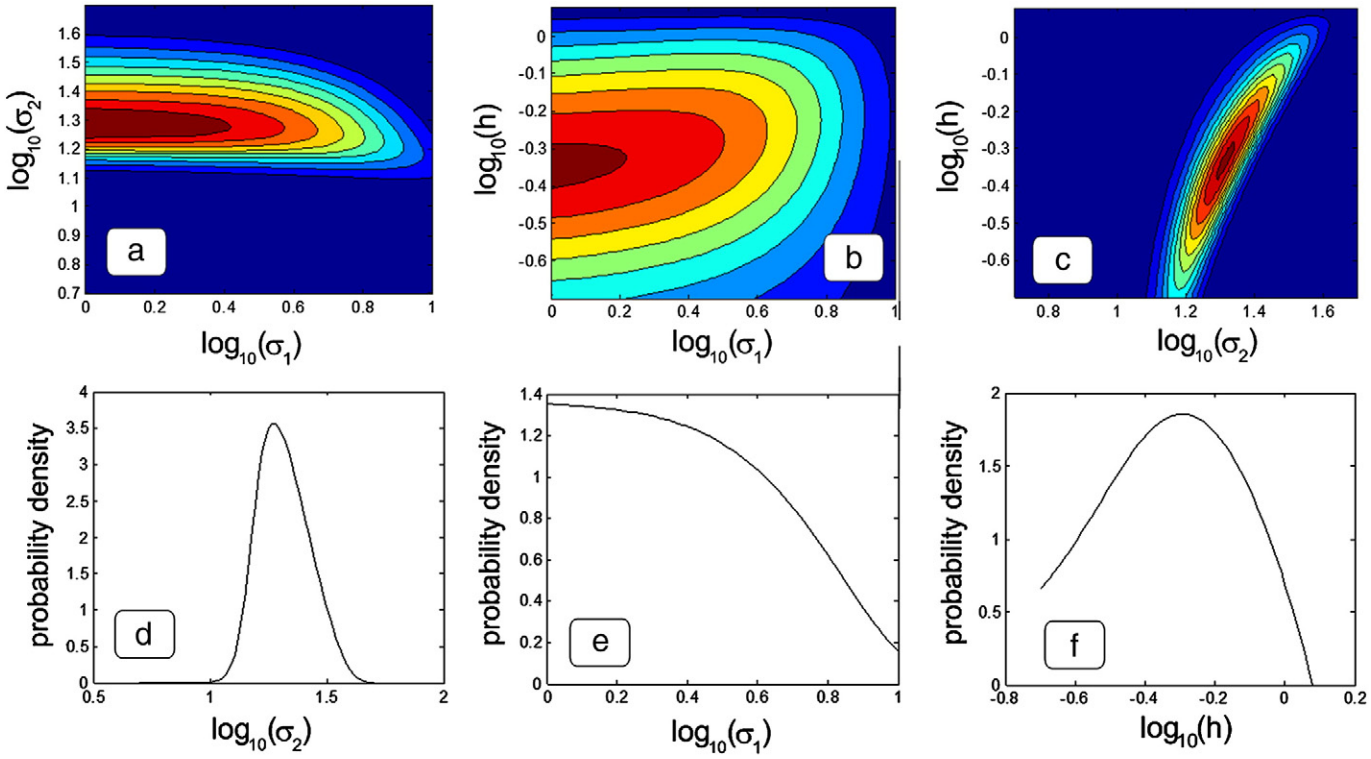

Fig. 5. Similar to Fig. 4, but including an a priori designed to limit the excursion of the parameter h related to the equivalence law.

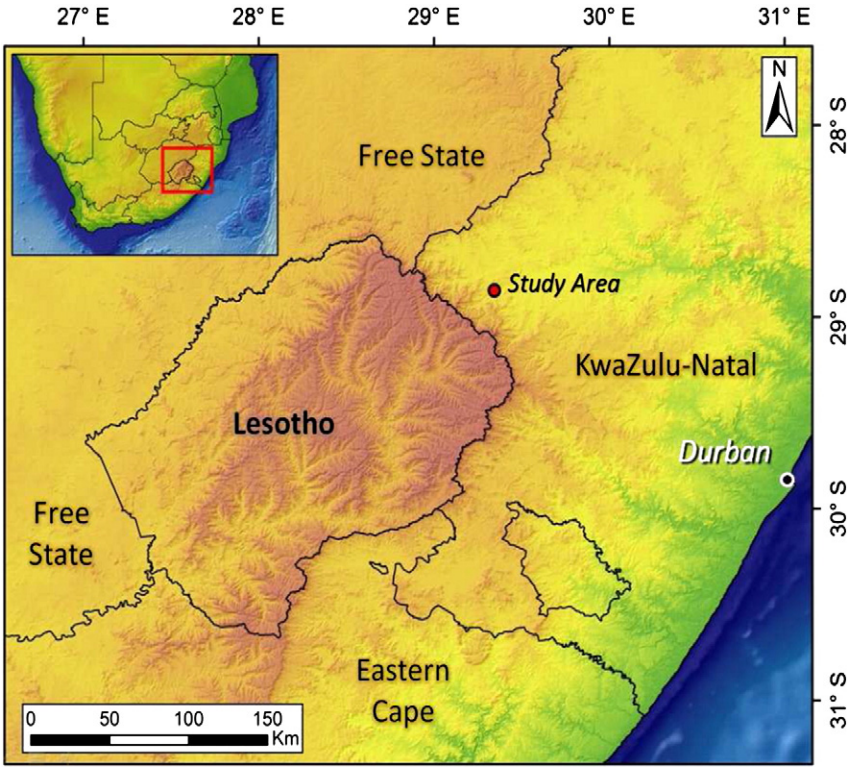

Fig. 6. Location of the site of Potshini in South Africa (adapted from Grellier et al., 2012b).

(here 40 cm in thickness), the subsoil Bt Horizon, in addition to the ongoing gully and tree encroachment problem.

5.3. Geophysical data

A 100 m × 150 m area was surveyed with an EM38-MK2 using a 5 m × 5 m sampling grid, and drift corrections were applied to the data, using the method described in Section 2.3. In this section we present the results obtained during the dry season, in the month of June 2010.

The resulting raw data maps are shown in Fig. 8.

Prior to the inversion process, it is useful to choose a model including any available a priori information. Firstly, the main features of the soil can be inferred simply by comparing the two VDM maps: the 1 m spacing data can be seen to be considerably more conductive than the 50 cm data, which means that within the first meter, the soil is likely to be composed of a resistive layer above a conductive layer.

Moreover, some information can be derived directly from field observations. The gully wall seen in Fig. 7 provides a good opportunity to make measurements and take samples from its face, although for

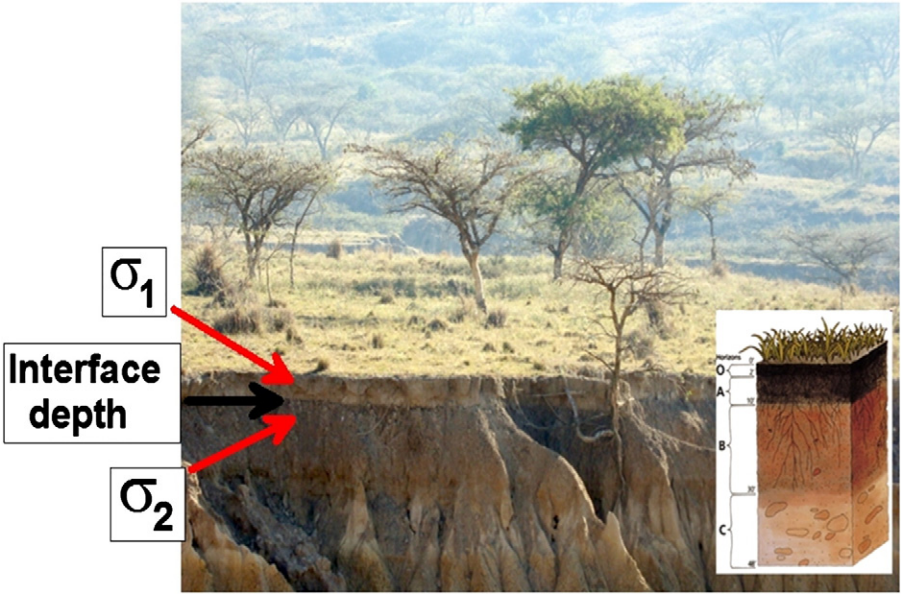

Fig. 7. Gully side-wall showing the soil horizons, in particular the A and B horizons, which are represented on the soil structure diagram shown at the bottom right of the figure. Courtesy of Wikipedia.

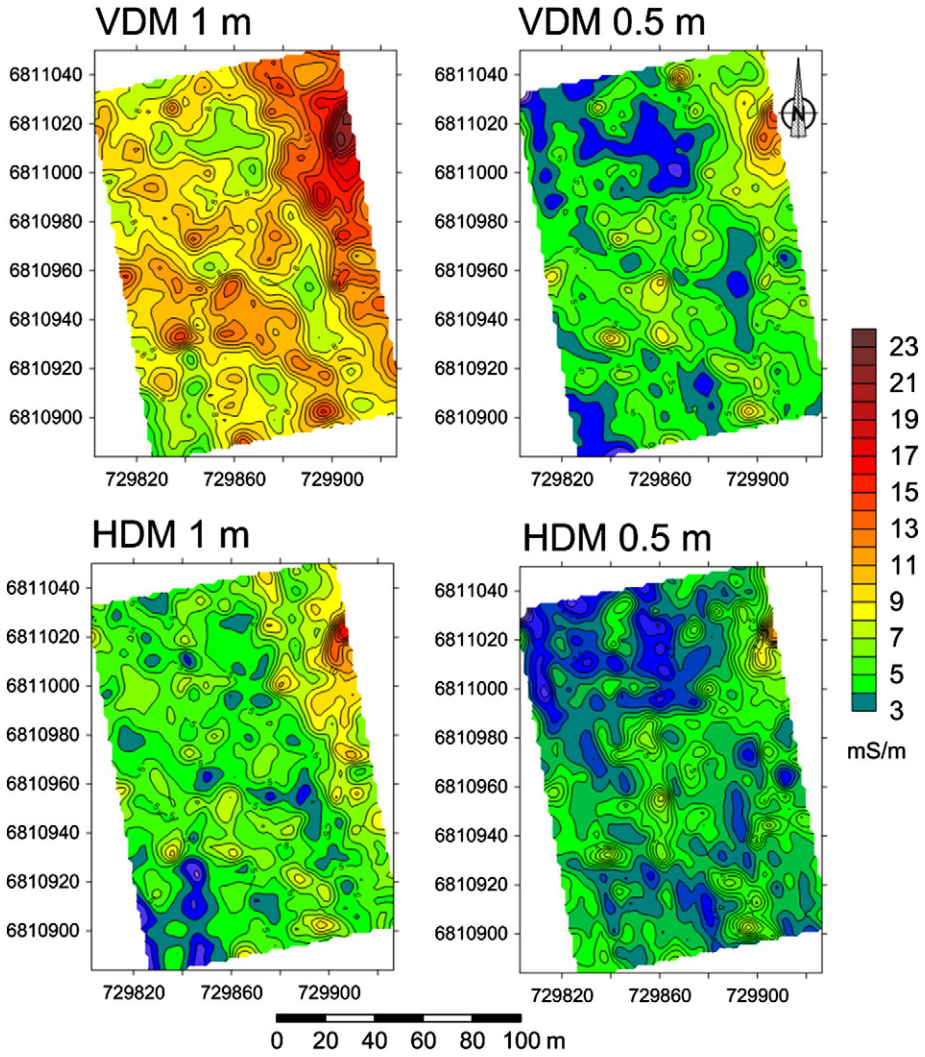

Fig. 8. Raw EM38-MK2 data in both VDM and HDM (vertical and horizontal dipole modes) with 50 cm and 1 m spacings. The color scale has been homogenized. The axes are shown in UTM coordinates.

reasons of security this could be achieved only down to a limited depth. Fig. 9 summarizes the data which was collected in this manner. The quantity of clay was derived from samples taken every 5 cm from a vertical log (the granulometric definition of clays, corresponding to particles less than two micrometers in diameter, is still used here). The resistivity was measured, also on the gully face, using a small pole–pole array (AM = 3 cm). Moreover, a Vertical Electrical Sounding (VES) was made at a distance of 4 m back from the gully face. All of the data obtained from these measurements confirmed the validity of the 2-layer horizontal structure of the ground, and confirmed that it was valid to perform further inversion by assuming a simple model, consisting of a non-conductive layer covering a clayey, more conductive layer.

Although the thickness of the topsoil layer in the gully section ranges between 40 cm and 50 cm, this parameter varies locally from 30 cm to 80 cm over the surveyed site.

5.4. Results from the Bayesian inversion and comparison with pit log data

The information described above can be used to adjust the a priori information. It combines multiplicatively the exploration window with a slight attractor which is used to prevent the extreme (and consequently the means too) values from drifting toward too high magnitudes made possible "within" the equivalence domain (see Eqs. (33) and (34)).

The a priori standard deviations of $(\sigma_a^V(s = 1\text{ m}); \sigma_a^V(s = 50\text{ cm}); \sigma_a^H(s = 1\text{ m}); \sigma_a^H(s = 50\text{ cm}))$ are: (2, 2, 3, 4) mS/m respectively. The error is assumed to be higher for the 50 cm spacing, due to a higher drift, and also because it is more difficult to hold the instrument flat on the ground at this scale, especially in the horizontal mode. The inverted parameters are mapped in Fig. 10.

From these maps we recomputed the data (in the data space). To do that, we first estimated the mean values of the parameters by successive marginal integration, and then we did a simple direct calculation. Notice that a full procedure would require to propagate first the whole PDF into the data space and then to integrate the resulting PDF in this space to get the mean values (and standard deviation). However, comparing the recomputed data obtained by the simpler procedure proposed above to the raw initial data leads to discrepancies not greater than the measurements errors. The RMS differences, that is $\text{RMS} = \sqrt{\frac{1}{n}\sum_{k=1}^{n}\left(d_k^{obs} - d_k^{cal}\right)^2}$, where d_k^{obs} and d_k^{cal} represent one observed parameter (for instance the VDM) and the same parameter as re-computed, respectively, were found:

VDM 1 m	→	1.4 mS/m
VDM 0.5 m	→	1.1 mS/m
HDM 1 m	→	1.4 mS/m
HDM 0.5 m	→	1.1 mS/m.

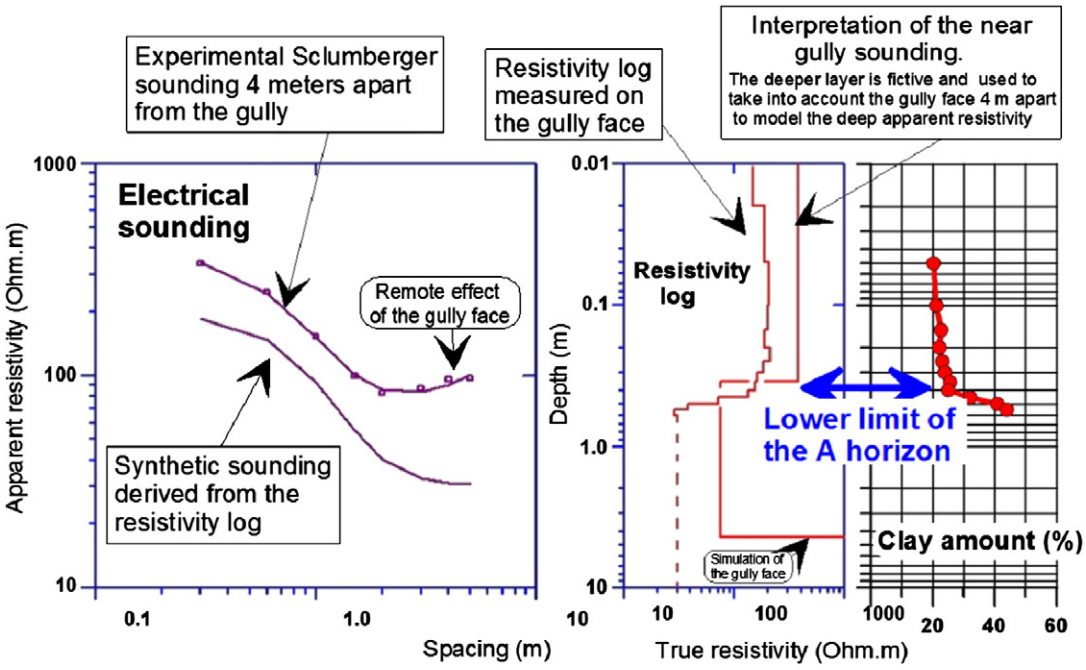

Fig. 9. Vertical electrical sounding close to the gully, and log profile of resistivity and clay percentage measured on the gully face. These recordings confirm the validity of the two-layer topsoil/subsoil used in the present study, as far as the geoelectric features are concerned.

In view of the fact that various systematic biases can affect the data (due mainly to drift effects), the noise levels used in the raw data appear to have been chosen realistically (2, 2, 3 and 4 mS/m respectively). By the way the found discrepancies are less than the assumed noise level, and this validates the simplified re-computing.

5.4.1. Comparison with conductivity and cation exchange capacity (CEC) data from pits

Four shallow pits allowed comparisons to be made with the "field reality". In each of these pits, we recorded the resistivity using a pole–pole array along the wall (AM = 3 cm). We also analyzed the mineralogical clay content by means of a CEC measurement, using the methylene blue (MB) technique (Cokca, and Birand, 1993; Hang and Brindley, 1970; Yukselen and Kaya, 2008). Both results are shown in Fig. 11. In addition, details of the MB method, which allows a MB titration to be converted to a CEC or a specific surface area, are provided in the appendix.

Pit B did not reach the clayey layer (cf. Figure 11). Despite some irregularities, the topsoil–subsoil interfaces determined from the conductivity and CEC (or clay percentage) measurements are in agreement. This is not surprising, since the clays are the cause of the high conductivities observed in this field. From these diagrams, and by averaging both curves, one can extract the interface depths at which there is a sudden increase in conductivity and CEC. These depths can be estimated as: A 45 cm; B >80 cm; C 50 cm; and D 60 cm. However, these limits remain fuzzy, and their small-scale variability (for lateral displacements of 10 cm or less) is not known.

The interface depths found in pits A, C, and D are in good agreement with those which can be read from Fig. 10, taking the errors bars into account (20% on h). In the case of B, the depth found in

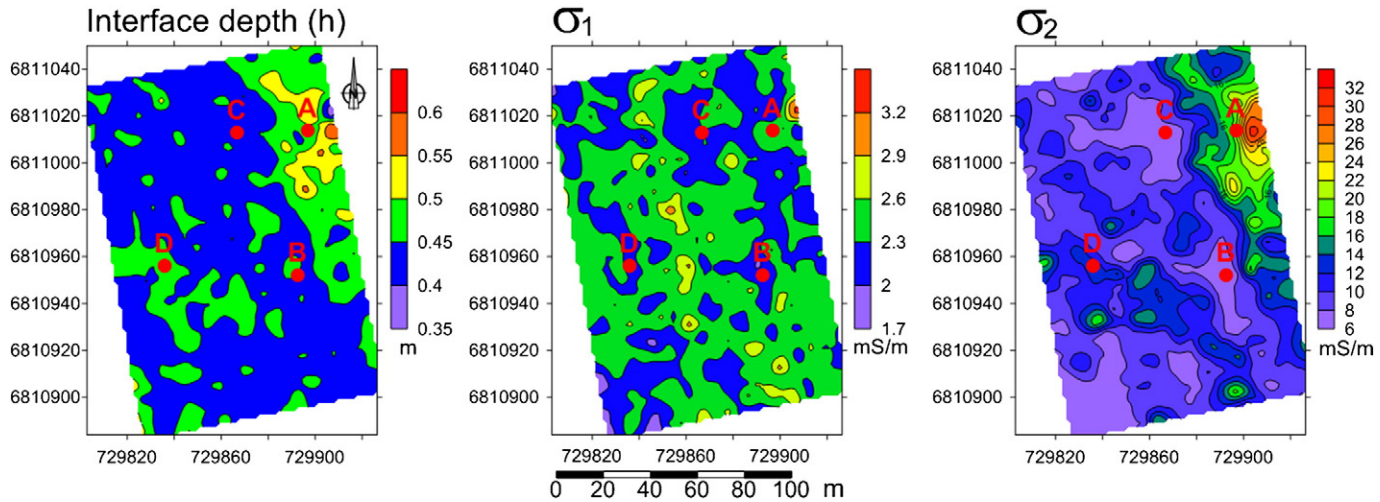

Fig. 10. Results of the Bayesian inversion. Points A, B, C and D indicate the position of validation pit logs, as discussed in the text. The uncertainties in this determination vary from approximately 20% for h (≈10 cm), to 25% for σ_1(≈0.6 mS/m), and 15% for σ_2(≈3 mS/m).

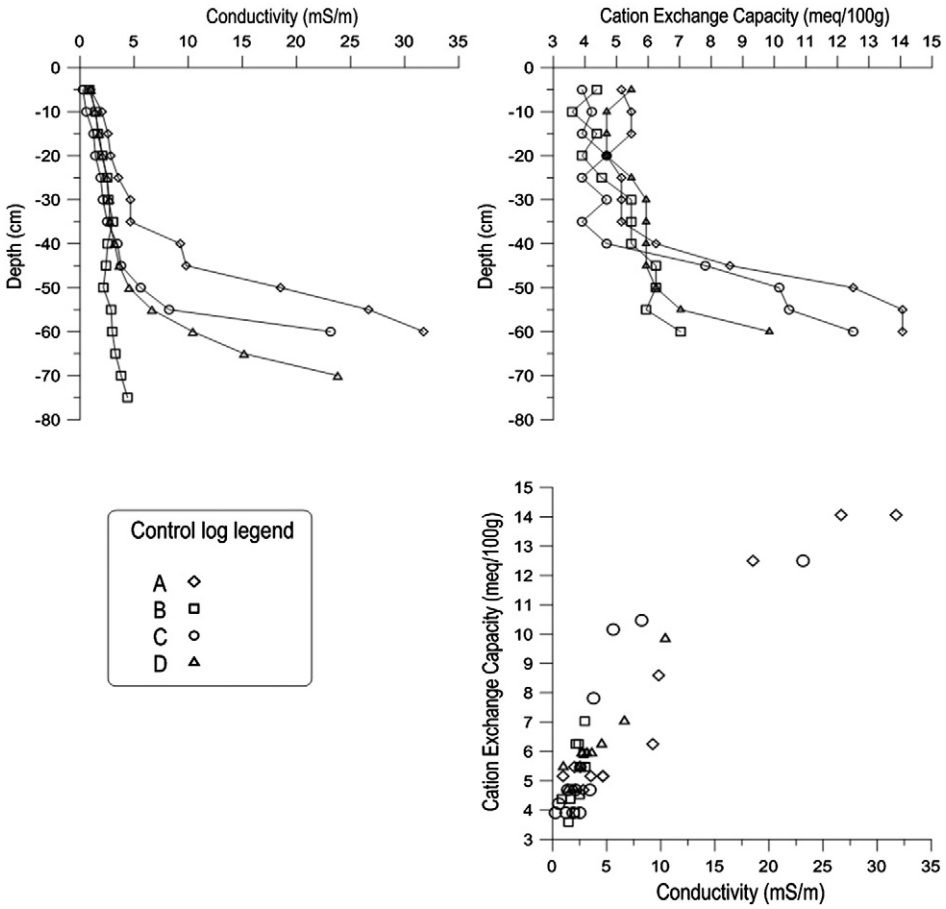

Fig. 11. Conductivity measured with a pole–pole array, and cation exchange capacity derived from the methylene blue method, in shallow control pits labeled A, B, C and D.

Fig. 10 is close to 50 cm, whereas the pit interface is not reached until a depth of 80 cm. However, the conductivity contrast is low at this location, making the uncertainty on h greater at this point, because the interface itself is not well defined. In such situations, where the interface depth cannot be constrained by the data, it is constrained by the a priori knowledge.

5.4.2. Application to tree encroachment in grassland

All of the tall trees (>3 m height) in the studied area were mapped using a differential global positioning system (DGPS) (Figure 12).

When the tree map (Figure 12) is compared with the σ_2 map (Figure 10), it can be seen that there are no trees in the areas of high conductivity (around pit A and pit D). The correlation observed here between tree densities and soil conductivities is consistent with the study of Robinson et al. (2010), for the case of oaks growing in semi-arid areas near to Stanford (California, USA). These authors showed that oaks growing in this savanna developed preferentially on soils with a lower conductivity in the first 1 m (~21 mS/m), associated with a lower clay content than in areas where only grass was present (~32 mS/m).

5.4.3. Discussion and conclusion

Tarantola and Valette clearly state that the PDF "is THE solution of the inverse problem". With this statement, they emphasized that the Bayesian process of propagating experimental field data through a physical law (also including the a priori information, or inversely) results in a solution which includes all of the information that can be retrieved from observations and a priori knowledge. In practice, in many situations it can be useful to provide only one value for the final parameter. For that purpose, the mathematical algorithm involves calculating the mean value of the parameter derived from the ultimate 1-D marginal probability. The Bayesian inversion has been shown to be totally robust, and allows correct management of the propagation of available information, from the data space to the parameter space. The complete process has been shown to work well on Slingram data, making it suitable for the quantitative interpretation of information related to the topsoil and subsoil that can be used in eco-geophysics for example. In this study, the Bayesian approach allows data to be inverted with a high reliability, and allows an analysis to be made in terms of information theory. Bayesian analysis can be used as a guide, to improve and simplify the exploitation of Slingram data for the retrieval of topsoil thickness and the conductivities of a two- (or more) layer model. In the present case (although a similar analysis could be efficient in another context), the outcome of the Bayesian analysis suggests that the interface depth remains close to 0.45 m, without varying significantly, and that the first horizon A has a low conductivity between 2 mS/m and 3 mS/m, with variations remaining within the error bar. If it is then considered that these parameters (first horizon thickness and conductivity) do not vary significantly, one could simplify the campaign by assuming that only the subsoil layer has a high and variable conductivity, which would allow just one measurement, for example the VDM with a 1 m spacing, to be made per point. The Bayesian approach proves that this would be sufficient, and beyond the inversion process described here, this result illustrates the most important contribution of the Bayesian method, i.e. that it provides an analysis of what has been done, and what can be done with the data, in terms of information content and management.

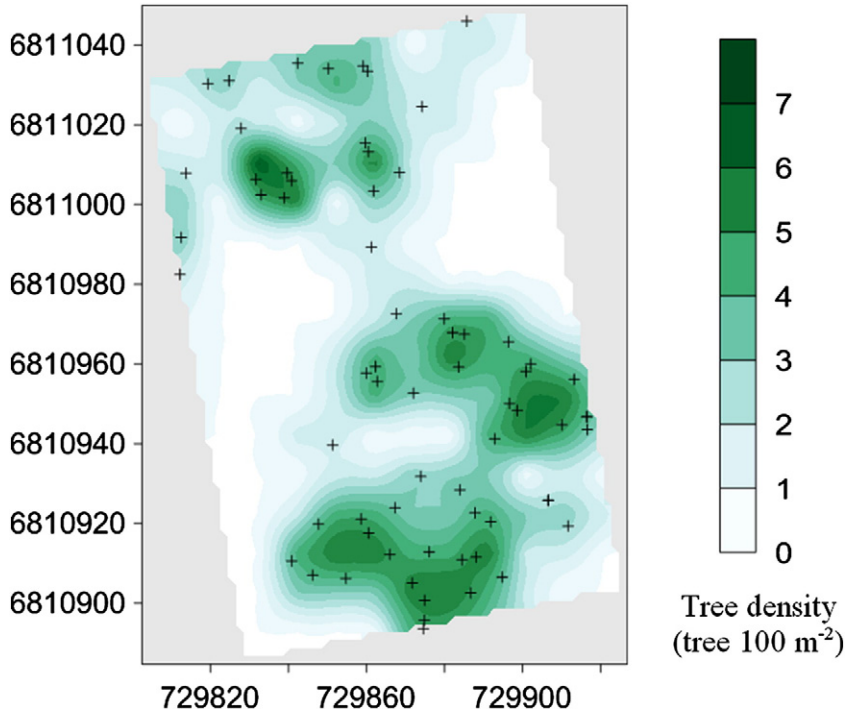

Fig. 12. Tall tree (>3 m in height) density map over a 1.5 ha area. Each tree is represented by a cross.

Acknowledgments

The authors would like to thank Gonca Okay, Myriam Schmutz, Pauline Ferry and John Ngeleka for their assistance. We further acknowledge the University of KwaZulu-Natal for the facilities provided during our study, and the Potshini community for the use of their land. This study has been made possible thanks to the facilities of the Institut de Recherche pour le Développement, France.

Appendix A. Methylene blue spot test

The soil's electrical conductivity (EC) (or its reciprocal, resistivity), when measured by geophysical methods, is directly related to its physico-chemical properties (Lesch and Corwin, 2003). Soil salinity, clay content, cation exchange capacity (CEC), clay mineralogy, soil pore size and distribution, and soil moisture (McNeill, 1992) can influence EC values.

The relationship between EC and soil properties can be described (for instance) by the formula given by Frohlich and Parke (1989), related to a modified Archie's law:

$$\sigma_0 = \frac{\sigma_{water}\Theta^k}{a} + \sigma_{surface} \quad (A1)$$

where σ_0 is the bulk conductivity of clayey material, a is a factor reflecting the influence of mineral grains on current flow, σ_{water} is the conductivity of pore water, Θ is the volumetric water content, and $\sigma_{surface}$ is the conductivity given by the surface of the clay particles. The parameter k is implicitly defined by:

$$\Theta^k = S_w^n \Phi^m \quad (A2)$$

where S_w is the degree of saturation, Φ is the porosity of the soil, and m is a material constant depending on the geometry of the pores, the degree of compaction, the mineral composition and the insulating properties of cementation (called the cementation factor).

This formula comprises a term related to the clay's properties, and a term related to the water content. The soil properties of the clayey material included in $\sigma_{surface}$, a and k thus play an important role in the value of the EC.

In order to validate the depth of the interface determined by inversion of the EM38-MK2 EC measurement data, the methylene blue spot method can be used to obtain a rapid, straightforward solution (Yukselen and Kaya, 2008). This method reveals some of the clay's properties (Hang and Brindley, 1970), and can allow, for example, the cation exchange capacity (CEC) (Kahr and Madsen, 1995), or the specific surface area (Santamarina et al., 2002), which should directly influence the EC, to be calculated.

The methylene blue (MB) molecule, $C_{16}H_{18}N_3S^+$, is a cationic dye which can adsorb onto negatively charged clay surfaces (Yukselen and Kaya, 2008). Its dimensions are: 1.7 nm × 0.76 nm × 0.32 nm, and the surface area covered by one molecule is approximately 1.3 nm^2 (Santamarina et al., 2002). By determining the quantity of methylene blue molecules which can be fixed onto the surface of clay particles in a specific soil, the clay properties of this soil can be determined. This easily applicable method is often used in geotechnical and construction work, in order to estimate the clay's resistance to water (swelling of clay).

The method used in the present study was as follows: soil samples were air dried and sieved with a 4 mm mesh. 30 g of the 0–4 mm soil fraction was mixed with 200 ml of de-ionized water. This soil suspension was continually mixed by a magnetic stirrer during the experiment. A MB solution was prepared by mixing 5 g of dry MB power with 500 ml of de-ionized water. The concentration of this solution was 10 g l^{-1}. The MB solution was then added by 5 ml increments to the soil suspension. A small drop was removed from the suspension 1 min following each addition of 5 ml of MB and placed onto filter paper, as shown in Fig. A1. A circle with a dark blue central zone, composed of soil aggregates, appears on the filter paper. If the unabsorbed MB forms a blue halo around the soil aggregate spot, a confirmation test is needed: a drop is removed from the suspension every minute, for a period of 5 min (with no further addition of MB); if the blue halo persists (after 5 drops), this means that the

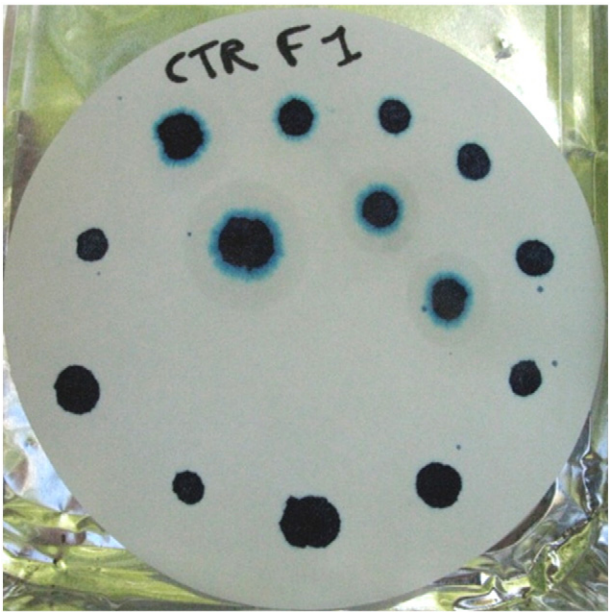

Fig. A1. Methylene blue spot test on one soil sample, with five of the spots having a permanent blue halo after five confirmation tests.

MB has replaced the cations in the double layer, and coated the entire surface area of the clay particles. If the blue halo disappears during the confirmation test, then the operator continues to add MB solution to the suspension. The CEC was calculated using the following formula (Cokca and Birand, 1993):

$$CEC = \frac{100}{m_s} V_{cc} N_{mb} \quad (A3)$$

where CEC is the cation exchange capacity ($cmol^{(+)}\ kg^{-1}$), m_S is the weight of the sample (g), V_{cc} is the volume of the MB titrant (mL), and N_{mb} is the normality of the MB substance (meq/mL), and

$$N_{mb} = \frac{w_{mb}}{320} \cdot \frac{100 - X}{100} \quad (A4)$$

where (w_{mb}) is the weight of the MB (g) and (X) is the moisture content of the MB substance (%).

References

Abdu, H., Robinson, D.A., Jones, S.B., 2007. Comparing bulk soil electrical conductivity determination using the DUALEM-1S and EM38-DD electromagnetic induction instruments. Soil Science Society of America Journal 71, 189–196. http://dx.doi.org/10.2136/sssaj2005.0394.

Archer, S., Schimel, D.S., Holland, E.A., 1995. Mechanisms of shrubland expansion: landuse, climate or CO_2. Climate Change 29, 91–95.

Bond, W.J., 2008. What limits trees in C_4 grasslands and savannas? Annual Review of Ecology, Evolution, and Systematics 39, 641–659.

Botha, G.A., Wintle, A.G., Vogel, J.C., 1994. Episodic late Quaternary palaeogully erosion in northern KwaZulu-Natal, South Africa. Catena 23, 327–340.

Brevik, E.C., Fenton, T.E., Lazari, A., 2006. Soil electrical conductivity as a function of soil water content and implications for soil mapping. Precision Agriculture 7, 393–404.

Burkinshaw, A.M., Bork, E.W., 2009. Shrub encroachment impacts the potential for multiple use conflicts on public land. Environmental Management 44, 493–504.

Carlin, B.P., Louis, T.A., 1998. Bayesian Methods for Data Analysis, Third Edition. Chapman & Hall/CRC Texts in Statistical Science (552pp, ISBN-10: 1584886978. ISBN-13: 9781584886976).

Cockx, L., Van Meirvenne, M., De Vos, B., 2007. Using the EM38DD soil sensor to delineate clay lenses in a sandy forest soil. Soil Science Society of America Journal 71, 1314–1322.

Cokca, E., Birand, A.A., 1993. Determination of cation exchange capacity of clayey soils by the methylene blue test. Geotechnical Testing Journal 16, 518–524.

Corwin, D.L., Lesch, S.M., 2005. Apparent soil electrical conductivity measurements in agriculture. Computers and Electronics in Agriculture 46, 11–43.

Deidda, G.P., Bonomi, E., Manzi, C., 2003. Inversion of electrical conductivity data with Tikhonov regularization approach: some considerations. Annals of Geophysics 46, 549–558.

Domsch, H., Giebel, A., 2004. Estimation of soil textural features from soil electrical conductivity recorded using the EM38. Precision Agriculture 5, 389–409. http://dx.doi.org/10.1023/B:PRAG.0000040807.18932.80.

Doolittle, J.A., Sudduth, K.A., Kitchen, N.R., Indorante, S.J., 1994. Estimating depths to claypans using electromagnetic induction methods. Journal of Soil and Water Conservation 49, 572–575.

Fernández-Martínez, J.L., García-Gonzalo, E., Saraswathi, S., Jernigan, R.L., Kloczkowski, A., 2011. Particle swarm optimization: a powerful family of stochastic optimizers. Analysis, design and application to inverse modelling. Lecture Notes in Computer Science 6728, 1–8. http://dx.doi.org/10.1007/978-3-642-21515-5_1.

Florsch, N., Hinderer, J., 2000. Bayesian estimation of the free core nutation parameters from the analysis of precise tidal gravity data. Physics of the Earth and Planetary Interiors 117, 21–35. http://dx.doi.org/10.1016/S0031-9201(99)00084-9.

Frohlich, R.K., Parke, C.D., 1989. The electrical resistivity of the vadose zone — field survey. Ground Water 27 (4), 524–530.

Ghorbani, A., Camerlynck, C., Florsch, N., Cosenza, P., Revil, A., 2007. Bayesian inference of the Cole–Cole parameters from time- and frequency-domain induced polarization. Geophysical Prospecting 55, 589–605.

Ghorbani, A., Camerlynck, C., Florsch, N., 2009. CR1Dinv: a Matlab program to invert 1D spectral induced polarization data for the Cole–Cole model including Electromagnetic effects. Computers & Geosciences 35, 255–266. http://dx.doi.org/10.1016/j.cageo.2008.06.001.

Grellier, S., Janeau, J.L., Barot, S., Ward, D., 2012a. Grass competition is more important than seed ingestion by livestock for Acacia recruitment in South Africa. Plant Ecology 213, 899–908.

Grellier, S., Kemp, J., Florsch, N., Janeau, J.L., Ward, D., Barot, S., Podwojewski, P., Lorentz, S., Valentin, C., 2012b. The indirect impact of encroaching trees on gully extension: a 64 year study in a sub-humid grassland of South Africa. Catena 98, 110–119.

Guy, R.M., Smith, J.M.B., 1995. N/A/95/12 A Land Potential Classification for KwaZulu-Natal.KwaZulu-Natal Department of Agriculture, Cedara, South Africa.

Hang, P.T., Brindley, G.W., 1970. Methylene blue absorption by clay minerals. Determination of surface areas and cation exchange capacities (clay-organic studies XVIII). Clays and Clays Minerals 18, 203–212.

Hanson, B.R., Kaita, K., 1997. Response of electromagnetic conductivity meter to soil salinity and soil water content. Journal of Irrigation and Drainage Engineering 123, 141–143.

Hendrickx, J.M.H., Borchers, B., Corwin, D.L., Lesch, S.M., Hilgendorf, A.C., Schlue, J., 2002. Inversion of soil conductivity profiles from electromagnetic induction measurements: theory and experimental verification. Soil Science Society of America Journal 66, 673–685.

Hezarjaribi, A., Sourell, H., 2007. Feasibility study of monitoring the total available water content using non-invasive electromagnetic induction-based and electrode-based soil electrical conductivity measurements. Irrigation and Drainage 56, 53–65.

Hossain, M.B., Lamb, D.W., Lockwood, P.V., Frazier, P., 2010. EM38 for volumetric soil water content estimation in the root-zone of deep vertosol soils. Computers and Electronics in Agriculture 74, 100–109.

Jeffreys, H., 1939. Theory of Probability.Clarendon Press, Oxford.

Jegen, M.D., Everett, M.E., Schultz, A., 2001. Using homotopy to invert geophysical data. Geophysics 66, 1749–1760. http://dx.doi.org/10.1190/1.1487117.

Kachanoski, R.G., De Jong, E., Van Wesenbeeck, I.J., 1990. Field scale patterns of soil water storage from non-contacting measurements of bulk electrical conductivity. Canadian Journal of Soil Science 70, 537–541.

Kahr, G., Madsen, F.T., 1995. Determination of the cation exchange capacity and the surface area of bentonite, illite and kaolinite by methylene blue adsorption. Applied Clay Science 9, 327–336.

Khakural, B.R., Robert, P.C., Hugins, D.R., 1998. Use of non-contacting electromagnetic inductive method for estimating soil moisture across a landscape. Communications in Soil Science and Plant Analysis 29, 2055–2065.

King, G.M., 2002. An Explanation of the 1:500 000 General Hydrogeological Map, Department of Water Affairs and Forestry, Pretoria, South Africa.

Kirkpatrick, S., Gelatt, C.D., Vecchi, M.P., 1983. Optimization by simulated annealing. Science New Series 220 (4598), 671–680. http://dx.doi.org/10.1126/science.220.4598.671 (ISSN 00368075. PMID 17813860. http://www.jstor.org/stable/1690046).

Kitchen, N.R., Sudduth, K.A., Drummond, S.T., 1996. Mapping of sand deposition from 1993 Midwest floods with electromagnetic induction measurements. Journal of Soil and Water Conservation 51, 336–340.

Kitchen, N.R., Sudduth, K.A., Drummond, S.T., 1999. Soil electrical conductivity as a crop productivity measure for claypan soils. Journal of Production Agriculture 12, 607–617.

Kitchen, N.R., Sudduth, K.A., Myers, D.B., Massey, R.E., Sadler, E.J., Lerch, R.N., Hummel, J.W., Palm, H.L., 2005. Development of a conservation-oriented precision agriculture system: crop production assessment and plan implementation. Journal of Soil and Water Conservation 60, 421–430.

Lesch, S.M., Corwin, D.L., 2003. Using the dual-pathway parallel conductance model to determine how different soil properties influence conductivity survey data. Agronomy Journal 95, 365–379.

Lesch, S.M., Strauss, D.J., Rhoades, J.D., 1995. Spatial prediction of soil salinity using electromagnetic induction techniques: II. An efficient spatial sampling algorithm suitable for multiple linear regression model identification and estimation. Water Resources Research 31, 87–398.

Lund, E.D., Christy, C.D., Drummond, P.E., 1999. Practical applications of soil electrical conductivity mapping in Precision Agriculture '99. In: Stafford, J.V. (Ed.), Proc. 2nd

European Conf. on Precision Agriculture. Sheffield Academic Press Ltd., Sheffield, UK, pp. 771–779.
McNeill, J.D., 1980. Electromagnetic terrain conductivity measurement at low induction numbers. Tech. Note TN-6. Geonics Ltd., Mississauga, Ontario (downloadable at http://www.geonics.com/pdfs/technicalnotes/tn6.pdf).
McNeill, J.D., 1992. Rapid, accurate mapping of soil salinity by electromagnetic ground conductivity meters. Advances in Measurement of Soil Physical Properties: Bringing Theory Into Practice. : Spec. Pub., 30. Soil Science Society of America, Madison, Wisconsin, pp. 209–229.
Menke, W., 1989. Geophysical Data Analysis: Discrete Inverse Theory. Academic Press, San Diego.
Mosegaard, K., Tarantola, A., 1995. Monte Carlo sampling of solutions to inverse problems. Journal of Geophysical Research 10 (B7), 12,431–12,447.
Mueller, T.G., Hartsock, N.J., Stombaugh, T.S., Shearer, S.A., Cornelius, P.L., Barnhisel, R.I., 2003. Soil electrical conductivity map variability in limestone soils overlain by loess. Agronomy Journal 95, 496–507.
Myers, D.B., Kitchen, N.R., Sudduth, K.A., Sharp, R.E., Miles, R.J., 2007. Soybean root distribution related to claypan soil properties and apparent soil electrical conductivity. Crop Science 47, 1498–1509.
Rhoades, J.D., Manteghi, N.A., Shrouse, P.J., Alves, W.J., 1989. Soil electrical conductivity and soil salinity: new formulations and calibrations. Soil Science Society of America Journal 53, 433–439.
Robinson, D.A., Lebron, I., Lesch, S.M., Shouse, P., 2004. Minimizing drift in electrical conductivity measurements in high temperature environments using the EM-38. Soil Science Society of America Journal 68, 339–345.
Robinson, D.A., Lebron, I., Querejeta, J.I., 2010. Determining soil–tree–grass relationships in a California oak savanna using eco-geophysics. Vadose Zone Journal 9, 1–8.
Saey, T., Simpson, D., Vitharana, U.W.A., Vermeersch, H., Vermang, J., Van Meirvenne, M., 2008. Reconstructing the paleotopography between the loess cover with the aid of an electromagnetic induction sensor. Catena 74, 58–64.
Saey, T., Simpson, D., Vermeersch, H., Cockx, L., Van Meirvenne, M., 2009. Comparing the EM38DD and DUALEM-21S sensors for depth-to-clay mapping. Soil Science Society of America Journal 73, 7–12.
Santamarina, J.C., Klein, K.A., Wang, Y.H., Prencke, E., 2002. Specific surface: determination and relevance. Canadian Geotechnical J. 39, 233–241.
Scales, J.A., Sneider, R., 1997. To Bayes or not to Bayes. Geophysics 62, 1045–1046.
Schenk, H.J., Jackson, R.B., 2002. Rooting depths, lateral root spreads and below-ground/above-ground allometries of plants in water-limited ecosystems. Journal of Ecology 90, 480–494.
Schleicher, J., Wiegand, K., Ward, D., 2011. Changes of woody plant interaction and spatial distribution between rocky and sandy soil areas in a semi-arid savanna, South Africa. Journal of Arid Environments 75, 270–278.
Scholes, R.J., Archer, S.R., 1997. Tree–grass interactions in savannas. Annual Review of Ecology and Systematics 28, 517–544.
Schulze, R.E., 1997. South African Atlas of Agrohydrology and Climatology. Water Research Commission, Pretoria, South Africa.
Sherlock, M.D., McDonnell, J.J., 2003. A new tool for hillslope hydrologists: spatially distributed groundwater level and soil water content measured using electromagnetic induction. Hydrological Process 17, 1965–1977.
Smit, G.N., 2004. An approach to tree thinning to structure southern African savannas for long-term restoration from bush encroachment. Journal of Environmental Management 71, 179–191.
Sudduth, K.A., Drummond, S.T., Kitchen, N.R., 2001. Accuracy issues in electromagnetic induction sensing of soil electrical conductivity for precision agriculture. Computers and Electronics in Agriculture 31, 239–264.
Sudduth, K.A., Kitchen, N.R., Myers, D.B., Drummond, S.T., 2010. Mapping depth to argillic soil horizons using apparent electrical conductivity. Journal of Environmental and Engineering Geophysics 15, 135–146. http://dx.doi.org/10.2113/JEEG15.3.135.
Tarantola, A., 2005. Inverse Problem Theory and Methods for Model Parameter Estimation. Society for Industrial and Applied Mathematics, Philadelphia, PA, USA. ISBN: 0898715725, p. 342.
Tarantola, A., 2006. Elements for Physics — Quantities, Qualities, and Instrinsic Theories. Springer, Albert Tarantola.
Tarantola, A., Valette, B., 1982a. Inverse problems—quest for information. Journal of Geophysics 50, 159–170.
Tarantola, A., Valette, B., 1982b. Generalized nonlinear inverse problem solved using the least square criterion. Reviews of Geophysics and Space Physics 20, 219–232.
Trelea, I.V., 2003. The particle swarm optimization algorithm: convergence analysis and parameter selection. Information Processing Letters 85, 317–325.
Triantafilis, J., Monteiro Santos, F.A., 2009. 2-Dimensional soil and vadose-zone representation using an EM38 and EM34 and a laterally constrained inversion model. Soil Research 47, 809–820. http://dx.doi.org/10.1071/SR09013.
Turner, B.L.I., Clark, W.C., Kates, R.W., Richards, J.F., Mathews, J.T., Meyers, W.B., 1990. The Earth as Transformed by Human Action. Cambridge University Press, New York.
Van Auken, O.W., 2009. Causes and consequences of woody plant encroachment into western north American grasslands. Journal of Environmental Management 90, 2931–2942.
Wiegand, K., Ward, D., Saltz, D., 2005. Multi-scale patterns and bush encroachment in an arid savanna with a shallow soil layer. Journal of Vegetation Science 16, 311–320.
Williams, B.G., Baker, G.C., 1982. An electromagnetic induction technique for reconnaissance surveys of soil salinity hazards. Australian Journal of Soil Research 20, 107–118.
Yukselen, Y., Kaya, A., 2008. Suitability of the methylene blue test for surface area, cation exchange capacity and swell potential determination of clayey soils. Engineering Geology 102, 38–45.